diamide's behavior on the basis of spectroscopic data should be more straightforward than for **1**. Previously reported variable-temperature ^{1}H NMR measurements ($\Delta\delta(NH)/\Delta T$) indicated that the intramolecularly hydrogen-bonded and non-hydrogen-bonded[6] states of **2** are of very similar enthalpy in CD_2Cl_2.[2a] In contrast, when an attempt was made to account for solvation by including three CH_2Cl_2 molecules in a "supermolecule" calculation, AM1 predicted the minimum energy intramolecularly hydrogen-bonded conformation of **2** to be 1.9 kcal/mol more enthalpically favorable than the minimum energy non-hydrogen-bonded conformation.[3]

In order to provide a more quantitative comparison with the calculations, we have now carried out an IR-based van't Hoff analysis of the intramolecular hydrogen bonding equilibrium occurring in a 1 mM CH_2Cl_2 solution of **2** over the temperature range −69 to 23 °C. Figure 1 shows the N–H stretch region of the IR spectra obtained at high and low temperatures. Both hydrogen-bonded (3340–50 cm^{-1}) and non hydrogen-bonded[6] (3443–8 cm^{-1}) bands are observed at each temperature. No hydrogen-bonded N–H stretch band can be detected at any temperature for a 1 mM sample of *N*-methylcyclohexylacetamide (**3**) in CH_2Cl_2; therefore, we used this compound to estimate the extinction coefficient of the non-hydrogen-bonded N–H stretch band of **2** as a function of temperature. van't Hoff analysis (intramolecularly hydrogen-bonded vs non-hydrogen-bonded states; each "state" comprises a set of conformations) indicated that the internally hydrogen-bonded state of **2** is 0.25 ± 0.06 kcal/mol less enthalpically favorable and 0.67 ± 0.48 eu more entropically favorable than the non-hydrogen-bonded state.[7]

Since CH_2Cl_2 is relatively nonpolar, it is interesting that *the internally hydrogen-bonded and non-hydrogen-bonded states of 2 have very similar enthalpies, with the state containing the N—H--O=C interaction slightly less enthalpically favorable.* An ideal amide–amide hydrogen bond should be enthalpically superior to any interaction between the amide group and the solvent. The enthalpic similarity of the internally hydrogen-bonded and non-hydrogen-bonded states of **2** may result from at least two factors: (1) the geometry of the seven-membered-ring hydrogen bond is not optimal for the amide–amide interaction (e.g., a nonlinear N–H--O angle is unavoidable); (2) closure of the hydrogen-bonded ring may involve the development of torsional strain and/or other enthalpically unfavorable interactions. The entropic similarity between the internally hydrogen-bonded and non-hydrogen-bonded states may arise from the fact that these two states enjoy similar degrees of conformational mobility[2c] and/or from desolvation associated with intramolecular hydrogen bond formation.[8] (The breadth and asymmetry of the hydrogen-bonded N–H stretch band in Figure 1 is consistent with the existence of multiple hydrogen-bonded ring conformations.)

Why does AM1 overestimate the enthalpic favorability of the intramolecularly hydrogen-bonded state of **2**? One potential source of error is indicated by the comparison between ab initio and AM1 results for the hydrogen-bonded formamide dimer reported by Novoa and Whangbo.[3] When interaction energy was examined as a function of the N–H--O angle, the ab initio calculations predicted that the hydrogen bond energy becomes increasingly unfavorable as the angle decreases below 150°.[9] For an N–H--O angle of 120° (the smallest angle examined), the ab initio interaction energy was 1.5 kcal/mol less favorable than in the 150–180° region. In contrast, AM1 predicted only small variations in interaction energy over the N–H--O angle range 120–180°, with a shallow minimum around 130°. (The ab initio results are in line with experimental observations concerning the geometric preferences of N—H--O=C hydrogen bonds.[10])

Since AM1 predictions for very simple systems are at odds with both experimental and ab initio results, it seems unlikely that AM1 calculations can provide useful insight on the behavior of triamide **1**. Indeed, the predicted minimum energy form of **1**·4(CH_2Cl_2) contains six- and seven-membered hydrogen-bonded rings, with N–H--O angles of 120° and 141°.[3,11]

Predicting the structural consequences stemming from the operation of complex networks of noncovalent interactions remains an important avenue of research.[1] The comparisons discussed here suggest that caution must be exercised in applying computational methods to such systems.

Acknowledgment. We thank Professor M.-H. Whangbo for sending manuscripts before publication and Professor William Saunders for helpful comments. This work was supported by the National Science Foundation (CHE-9014488). G.P.D. is the recipient of a National Research Service Award (T32 GM08923) from the National Institute of General Medical Sciences. S.H.G. is grateful to the Searle Scholars Program, the NSF PYI Program (CHE-9157510), the Eastman Kodak Company, and the Upjohn Company for support. The FT-IR spectrometer was purchased with funds provided by the Office of Naval Research (N00014-90-1902).

Supplementary Material Available: Representative van't Hoff plot for intramolecular hydrogen bonding of **2** in CH_2Cl_2 (1 page). Ordering information is given on any current masthead page.

(6) We use the term "non-hydrogen-bonded" to signify the absence of an N—H--O=C interaction. Such protons are presumably engaged in weak interactions with the solvent.

(7) A representative van't Hoff plot is included as supplementary material. Only the non-hydrogen-bonded N–H stretch band was used for quantification, because appropriate reference compounds were not available for determining the extinction coefficient of the hydrogen-bonded N–H stretch band. We have previously shown that this type of IR-based van't Hoff analysis of intramolecular hydrogen bonding in simple diamides provides results quantitatively similar to those of ^{1}H NMR-based van't Hoff analysis; see ref 2c.

(8) For a dramatic example of solvation effects on noncovalent association phenomena in CD_2Cl_2, see: Bryant, J. A.; Knobler, C. B.; Cram, D. J. *J. Am. Chem. Soc.* **1990**, *112*, 1254.

(9) See Figure 2a of ref 3.

(10) (a) Baker, E. N.; Hubbard, R. E. *Prog. Biophys. Mol. Biol.* **1984**, *44*, 97 and references therein. (b) Taylor, R.; Kennard, O.; Versichel, W. *Acta Crystallogr.* **1984**, *B40*, 280.

(11) Geometrically problematic hydrogen-bonding predictions by AM1 have been reported previously: (a) Rzepa, H. S.; Yi, M. *J. Chem. Soc., Perkin Trans. 2* **1991**, 531 and references therein. (b) Schröder, S.; Daggett, V.; Kollman, P. *J. Am. Chem. Soc.* **1991**, *113*, 8922.

Diffusion-Ordered Two-Dimensional Nuclear Magnetic Resonance Spectroscopy

Kevin F. Morris and Charles S. Johnson, Jr.*

Department of Chemistry, University of North Carolina Chapel Hill, North Carolina 27599-3290

Received December 9, 1991

A noninvasive analytical method is needed that can identify molecular components of mixtures *and* simultaneously characterize the sizes of aggregates and other structures present. Consider, for example, a broth containing vesicles, micelles, and protein fragments. Light-scattering experiments cannot resolve such mixtures, and chromatographic methods may disrupt fragile structures such as micelles and vesicles. In any case hydrodynamic methods typically do not directly identify the molecular components. Even highly selective NMR methods are at a disadvantage with mixtures of species having complicated spectra. Here we report an alternative analysis method, a 2D-NMR experiment that displays an NMR chemical shift spectrum in one direction and a "spectrum" of diffusion coefficients or particle sizes in the other, i.e., for each radius the NMR spectrum of associated molecular species is displayed. This experiment complements existing analytical methods and provides a global view of particle sizes in the sample. It is effective at detecting impurities and aggregates in samples and, furthermore, is relatively easy to implement on modern NMR spectrometer systems.

* Author to whom correspondence should be addressed.

0002-7863/92/1514-3139$03.00/0

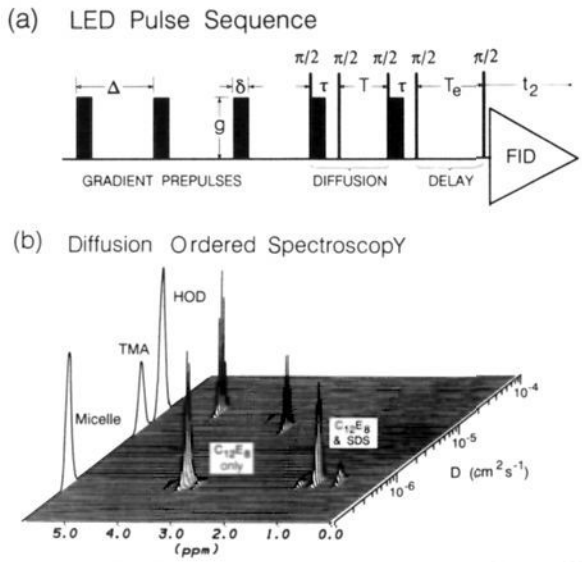

Figure 1. (a) The LED pulse sequence. Note that $\Delta = T + \tau$. Homospoil pulses during the interval T_e and phase cycling of the rf pulses are not shown. (b) The diffusion-ordered 2D-NMR spectrum of a sample containing TMA and mixed micelles in D_2O.

Basically, NMR spectra are obtained with the FT pulsed field gradient method,[1] and data sets are collected as the gradient pulse areas are incremented through approximately 50 values. Then powerful data inversion programs are used to generate diffusion spectra at each chemical shift. Through the use of the LED[2] pulse sequence illustrated in Figure 1a and actively shielded gradient coils,[3,4] large gradient amplitudes (>300 G/cm) can be accommodated and tracer diffusion coefficients spanning 5 orders of magnitude with a lower limit of less than 10^{-10} cm^2 s^{-1} can be measured. We call this experiment diffusion-ordered 2D-NMR spectroscopy (DOSY), and we recall Stilbs's suggestion that "size resolved NMR" could be based on diffusion-related echo attenuation.[1,5] Mobility ordered NMR spectroscopy (MOSY), in which electrophoretic mobilities are displayed at each chemical shift, is a closely related technique.[6]

The NMR spectrum, obtained by Fourier transformation with respect to t_2, can be represented by

$$I(K,\omega) = \sum_i I_{oi}(\omega) R_i(\tau,\Delta,T_e) \exp[-D_i K^2(\Delta - \delta/3)] \quad (1)$$

where $I_{oi}(\omega)$ is the 1D spectrum of the ith diffusing species, $R_i(\tau,T,T_e) = \exp[-2\tau/T_2^i - (T + T_e)/T_1^i]$ is a relaxation factor, and T_2^i and T_1^i are nuclear transverse and longitudinal relaxation times, respectively. D_i is the tracer diffusion coefficient of the ith species, and $K = \gamma g \delta$ is the pulse area where g and δ are the amplitude and duration of a gradient pulse, respectively. Thus at each chemical shift ω the NMR signal as a function of K^2 is a sum of decaying exponentials. This sum can be inverted to yield a spectrum of diffusion rates;[7] however, the problem is ill-posed and often intractable.[8,9] Fortunately, robust algorithms have been developed that will either perform the analysis or report inadequate data. DISCRETE[9,10] and CONTIN[11,12] are widely distributed programs that handle discrete and continuous distributions of diffusion coefficients, respectively. These or similar programs can be incorporated into the NMR analysis programs to generate the diffusion dimension.

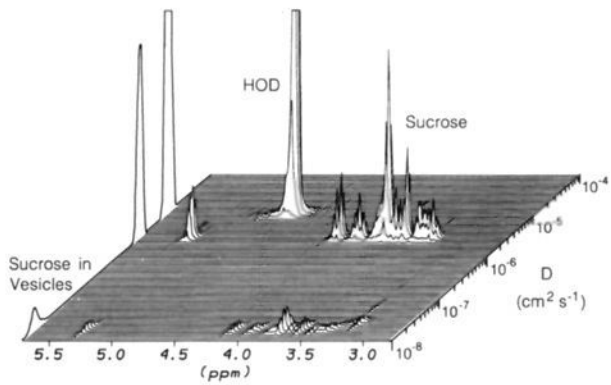

Figure 2. The diffusion-ordered 2D-NMR spectrum of a sample containing sucrose and phospholipid vesicles in D_2O.

Figure 1b shows the DOSY spectrum for a sample containing 10.0 mM tetramethylammonium chloride (TMA) with mixed micelles [4.00 mM sodium dodecyl sulfate (SDS) and 8.00 mM octaethylene glycol dodecyl ether ($C_{12}E_8$)]. The ^{1}H spectra were obtained at 295 K with a Brüker AC-250 spectrometer with custom-built probe and gradient driver.[13] The time intervals (Figures 1a and 2) were Δ = 100.0 ms, $\tau - \delta$ = 0.500 ms, and T_e = 100.0 ms, and 38 NMR spectra were collected at values of K ranging from 144 to 8.19 × 10^3 cm^{-1}. Fourier transformations were performed with the NMR software package FELIX (Hare Research, Incorporated), and then each column in the 2D data set was analyzed by DISCRETE on a SGI INDIGO computer. Diffusion spectra were synthesized from Gaussian components with center positions and intensities corresponding to the decay rates and amplitudes given by DISCRETE's best fit. The line widths were set equal to either the standard deviation σ_i determined by DISCRETE or a predetermined minimum value, chosen to compensate for small differences in decay rates at different chemical shifts so as to insure a smooth projection on the diffusion axis. The sets of surfactant peaks in the spectral regions 3.78–3.25 ppm and 1.40–0.69 ppm occur at the same position in the diffusion dimension, indicating that they are both associated with the micelle. The diffusion coefficients obtained for HOD, TMA, and the mixed micelle are 1.21 × 10^{-5}, 7.89 × 10^{-6}, and 5.54 × 10^{-7} cm^2 s^{-1}, respectively.

Figure 2 provides an illustration of DOSY for sucrose in the presence of phospholipid vesicles. Vesicles consist of a bilayer in the form of a spherical shell that encloses an aqueous region in which materials can be entrapped. Here large unilamellar vesicles were prepared by an extrusion technique,[14] with a solution that was initially 100 mM 1-palmitoyl-2-oleoyl phosphatidylcholine (Avanti Polar Lipids, Inc.), 100 mM sucrose, and 100.0 mM NaCl. Thirty-nine NMR spectra were collected with K values ranging from 289 to 2.62 × 10^4 cm^{-1}. The diffusion peaks for free sucrose and sucrose entrapped in the vesicles are easily resolved with diffusion coefficients of 3.00 × 10^{-6} and 1.86 × 10^{-8} cm^2 s^{-1}, respectively; and the intense HOD peak at 1.24 × 10^{-5} cm^2 s^{-1} is clearly separated from the sucrose peaks. Note that phospholipid bilayers are highly permeable to water but not sucrose. The phospholipid headgroup peak at 3.10 ppm gives evidence of orientational effects, in agreement with recent 1D PFG-NMR experiments on large phospholipid vesicles, complete details of which will be presented elsewhere.[15]

The DISCRETE analysis used here requires no initial knowledge of the number of components or the values of parameters and thus permits automated implementation of the analysis for large data

(1) Stilbs, P. *Prog. NMR Spectrosc.* **1987**, *19*, 1.
(2) Gibbs, S. J.; Johnson, C. S., Jr. *J. Magn. Reson.* **1991**, *93*, 395.
(3) Mansfield, P.; Chapman, B. *J. Magn. Reson.* **1986**, *66*, 573.
(4) Gibbs, S. J.; Morris, K. F.; Johnson, C. S., Jr. *J. Magn. Reson.* **1991**, *94*, 165.
(5) Stilbs, P. *Anal. Chem.* **1981**, *53*, 2135.
(6) Morris, K. F.; Johnson, C. S., Jr. *J. Am. Chem. Soc.* **1992**, *114*, 776.
(7) Gardner, D. C.; Gardner, J. C.; Laush, G.; Meinke, W. W. *J. Chem. Phys.* **1959**, *31*, 978.
(8) Lanczos, C. *Applied Analysis*; Prentice Hall: Englewood Cliffs, 1956; p 272.
(9) Provencher, S. W. *J. Chem. Phys.* **1976**, *64*, 2772.
(10) Provencher, S. W. *Biophys. J.* **1976**, *16*, 27.
(11) Provencher, S. W. *Comput. Phys. Commun.* **1982**, *27*, 213.
(12) Provencher, S. W. *Comput. Phys. Commun.* **1982**, *27*, 229.
(13) Saarinen, T. R.; Woodward, W. S. *Rev. Sci. Instrum.* **1988**, *59*, 761.
(14) He, Q.; Hinton, D. P.; Johnson, C. S., Jr. *J. Magn. Reson.* **1991**, *91*, 654.
(15) Hinton, D. P.; Johnson, C. S., Jr. *Book of Abstracts*; 32nd Experimental NMR Conference, St. Louis, MO; p 77 and data to be published.

sets. Analyses of multiexponential decays with three or more components and with decay rates differing by less than a factor of 2 may fail. However, accessible diffusion coefficients range over 4 orders of magnitude, and usually only one or two diffusing components are encountered at a given chemical shift. DOSY is especially good for complex mixtures having a large range of particle sizes, e.g., proteins with cofactors and microemulsion systems. For polydisperse systems, DISCRETE can be replaced by CONTIN, as is common in dynamic light scattering applications, to obtain the distribution of diffusion rates and, through the Stokes-Einstein relation, particle sizes.[16] Also, accuracy and consistency can be improved by incorporating programs that can simultaneously transform data for a range of chemical shifts. DOSY is expected to be widely accessible to chemists because of currently available gradient accessories for NMR systems, inexpensive computer workstations, and freely distributed software. We note in closing that DOSY is a special case of "relaxation resolved spectroscopy", a point that will be explored elsewhere for other nuclear spin relaxation processes.

Acknowledgment. This work was supported in part under National Science Foundation Grant CHE-8921144. We thank Ms. D. P. Hinton for advice and for supplying phospholipid vesicle samples.

(16) For an introduction to analysis methods, see: Chu, B. *Laser Light Scattering*, 2nd ed.; Academic Press: Boston, 1991; Chapter VII.

Synthesis of Pure $^{13}C_{60}$ and Determination of the Isotope Effect for Fullerene Superconductors

Chia-Chun Chen and Charles M. Lieber*

Department of Chemistry and Division of Applied Sciences, Harvard University Cambridge, Massachusetts 02138

Received January 27, 1992

Herein we report the synthesis of 99% $^{13}C_{60}$ and the measurement of the isotope effect on the superconducting transition temperature (T_c) in potassium-doped materials. To our knowledge, this work represents the first preparation of isotopically pure material and has thus enabled an unambiguous analysis of the isotope shift. Our results demonstrate that T_c is depressed significantly in $K_3{}^{13}C_{60}$ versus $K_3{}^{12}C_{60}$. The depression of T_c for the ^{13}C material indicates that superconductivity arises from phonon-mediated pairing and is not purely electronic in origin.[1,2] The value of the isotope exponent, $\alpha = 0.3$ ($T_c \propto M^{-\alpha}$), is smaller than the theoretical prediction of $\alpha = 0.5$ for a simple phonon mechanism[3] and therefore also suggests that other interactions play a role in determining superconductivity in these cluster-based solids.

Several methods have been used to prepare C_{60} enriched with ^{13}C. One technique involves packing hollow carbon-12 rods with ^{13}C powder and then resistively vaporizing the rods to produce a distribution of $^{13}C/^{12}C$ fullerenes.[4] More recently, Ramirez et al. prepared carbon rods from a mixture of carbon-13 powder and [^{13}C]glucose, but found significant ^{12}C incorporated into the C_{60} product.[5] Pure $^{13}C_{60}$ and not a distribution of $^{13}C/^{12}C$ is needed, however, to determine unambiguously the isotope effect on T_c and other physical properties.

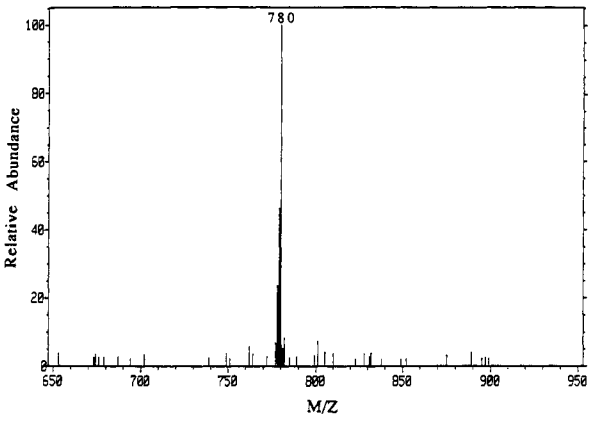

Figure 1. Field desorption (FD) mass spectrum of a purified $^{13}C_{60}$ sample (M^+, 780) recorded using a JEOL AX505H spectrometer. Experimental conditions were as follows: 30 mA FD emitter current; 3 keV ion energy; 9 keV extraction energy. Similar spectra were recorded using fast atom bombardment.

Table I. Experimental and Calculated Infrared Absorption Bands for $^{12}C_{60}$ and $^{13}C_{60}$

	frequency (cm^{-1})			
$^{12}C_{60}$ (exptl)	1429	1183	576	527
$^{13}C_{60}$ (calcd[a])	1373	1137	553	506
$^{13}C_{60}$ (exptl)	1375	1138	554	506

[a] Calculated from the $^{12}C_{60}$ experimental data using $\nu(^{13}C_{60}) = \nu(^{12}C_{60})[M(^{12}C)/M(^{13}C)]^{1/2}$. IR spectra were recorded on C_{60} thin films using a Nicolet-5PC FT-IR.

To obtain $^{13}C_{60}$ we prepare isotopically pure carbon-13 rods using a straightforward method that can be carried out with standard equipment. First, ^{13}C powder (99% ^{13}C, Aldrich) was placed in a 0.125-in. i.d. quartz tube between two tantalum rods, and then this assembly was evacuated to ca. 10^{-2} Torr. A constant pressure of 2000 lbs/in^2 was applied using a laboratory press while current pulses (10 A, 2-3 s) were passed through the sample to drive out air and water. The carbon rods were then formed by sequentially increasing the applied current while the powder was under compression. We found that a sequence of 10-, 50-, and 100-A currents, each applied for 10 s, resulted in the formation of high-quality rods. The rods fabricated in this way were 10-15 mm long and similar in density to commercial ^{12}C rods. The ^{13}C rods were resistively vaporized,[6,7] and pure $^{13}C_{60}$ was isolated from the resulting carbon soot by chromatography, as discussed previously.[8,9]

Figure 1 shows the field desorption mass spectrum of purified $^{13}C_{60}$. The M^+ signal is at m/z 780. The ions at m/z 779 and 778 are isotope peaks resulting from the presence of 1% ^{12}C in the starting material. Since essentially no signal is observed above the background level from m/z 700-777, we can conclude that our material is not contaminated with $^{12}C_{60}$. Furthermore, no signal was detected at m/z 910 (mass $^{13}C_{70}$ = 910) in spectra recorded on purified $^{13}C_{60}$ samples. ^{13}C NMR spectra (Brucker AM-500) obtained in C_6D_6 showed the single peak at 143.2 ppm expected for $^{13}C_{60}$;[4] no resonances were detected for $^{13}C_{70}$. In

(1) (a) Chakravarty, S.; Gelfand, M. P.; Kivelson, S. *Science* **1991**, *254*, 970. (b) Chakravarty, S.; Kivelson, S. *Europhys. Lett.* **1991**, *16*, 751.

(2) (a) Varma, C. M.; Zaanen, J.; Raghavachari, K. *Science* **1991**, *254*, 989. (b) Schluter, M. A.; Lannoo, M.; Needels, M.; Baraff, G. A. Submitted for publication.

(3) Bardeen, J.; Cooper, L. N.; Schrieffer, J. R. *Phys. Rev.* **1957**, *108*, 1175.

(4) (a) Johnson, R. D.; Meijer, G.; Salem, J. R.; Bethune, D. S. *J. Am. Chem. Soc.* **1991**, *113*, 3619. (b) Hawkins, J. M.; Loren, S.; Meyer, A.; Nunlist, R. *J. Am. Chem. Soc.* **1991**, *113*, 7770.

(5) Ramirez, A. P.; Kortan, A. R.; Rosseinsky, M. J.; Duclos, S. J.; Mujsce, A. M.; Haddon, R. C.; Murphy, D. W.; Makhija, A. V.; Zahurak, S. M.; Lyons, K. B. *Phys. Rev. Lett.* **1992**, *68*, 1058.

(6) Kratschmer, W.; Lamb, L. D.; Fostiropoulos, K.; Huffman, D. R. *Nature* **1990**, *347*, 354.

(7) Haufler, R. E.; Conceicao, J.; Chibante, L. P. F.; Chai, Y.; Byrne, N. E.; Flanagan, S.; Haley, M. M.; O'Brien, S. C.; Pan, C.; Xiao, Z.; Billups, W. E.; Ciufolini, M. A.; Hauge, R. H.; Margrave, J. L.; Wilson, L. J.; Curl, R. F.; Smally, R. E. *J. Phys. Chem.* **1990**, *94*, 8634.

(8) Diederich, F.; Ettl, R.; Rubin, Y.; Whetten, R. L.; Beck, R.; Alvarez, M.; Anz, S.; Sensharma, D.; Wudl, F.; Khemani, K. C.; Koch, A. *Science* **1991**, *252*, 548.

(9) Chen, C.-C.; Kelty, S. P.; Lieber, C. M. *Science* **1991**, *253*, 886.

0002-7863/92/1514-3141$03.00/0